Inorganic Chemistry

Article

pubs.acs.org/IC

α-Amino Acid Derived Benzimidazole-Linked Rhodamines: A Case of Substitution Effect at the Amino Acid Site toward Spiro Ring Opening for Selective Sensing of Al^{3+} Ions

Anupam Majumdar,[†] Subhendu Mondal,[†] Constantin G. Daniliuc,[‡] Debashis Sahu,[§] Bishwajit Ganguly,*[,§] Sourav Ghosh,[∥] Utpal Ghosh,[∥] and Kumaresh Ghosh*[,†]

[†]Department of Chemistry, University of Kalyani, Kalyani 741235, India

[‡]Organisch-Chemisches Institut, Universität Münster, Corrensstrasse 40, 48159 Münster, Germany

[§]Computation and Simulation Unit (Analytical Discipline and Centralized Instrument Facility), CSIR-Central Salt and Marine Chemicals Research Institute, Bhavnagar, Gujarat 364002, India

[∥]Department of Biochemistry & Biophysics, University of Kalyani, Kalyani 741235, India

Supporting Information

ABSTRACT: α-Amino acid derived benzimidazole-linked rhodamines have been synthesized, and their metal ion sensing properties have been evaluated. Experimentally, L-valine- and L-phenylglycine-derived benzimidazole-based rhodamines **1** and **2** selectively recognize Al^{3+} ion in aqueous CH_3CN (CH_3CN/H_2O 4/1 v/v, 10 mM tris HCl buffer, pH 7.0) over the other cations by exhibiting color and "turn-on" emission changes. In contrast, glycine-derived benzimidazole **3** remains silent in the recognition event and emphasizes the role of α-substitution of amino acid undertaken in the design. The fact has been addressed on the basis of the single-crystal X-ray structures and theoretical calculations. Moreover, pink **1**·Al^{3+} and **2**·Al^{3+} ensembles selectively sensed F^- ions over other halides through a discharge of color. Importantly, compounds **1** and **2** are cell permeable and have been used as imaging reagents for the detection of Al^{3+} uptake in human lung carcinoma cell line A549.

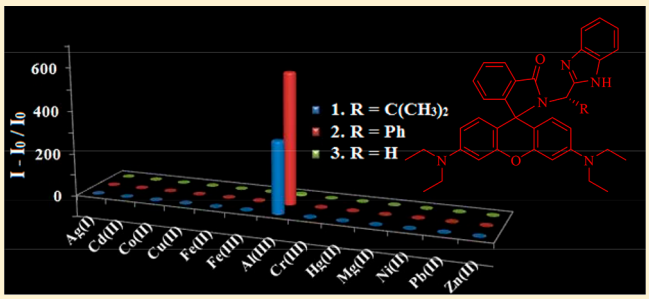

INTRODUCTION

The design and synthesis of optical signaling systems based on organic scaffolds for sensing and recognition of biologically and environmentally important metal ions has attracted a great deal of attention.[1] Optical cation sensors, where the interaction with a cation leads to a change in the absorbance (color) or fluorescence properties of the receptor, are the most widely suitable class of cation sensors. Fluorometric and colorimetric methods for sensing of metal ions are important tools due to the operational simplicity and low detection limits.[2] As a fluorophore and chromophore, the rhodamine fluorochrome has drawn the attention of chemists to develop sensors due to its excellent photophysical properties and, in this regard, various rhodamine-based fluorescent probes for cations, anions, and other analytes have been reported.[3] In spite of significant reports on rhodamine-based molecular probes for metal ions, the use of amino acid derived benzimidazole-based rhodamines in this capacity are unknown.

Our continued interest in ion sensing[4] inspired us to develop α-amino acid derived benzimidazole-linked rhodamine molecules **1**−**3** for metal ion sensing, both colorimetrically and fluorimetrically. Structural analysis of the compounds reveals that all three compounds are structurally the same. There is only a difference in substituents of the amino acid derived benzimidazoles which corroborate different sensing behaviors toward metal ions. While compounds **1** and **2** are fluorometrically and colorimetrically sensitive to Al^{3+} ions in aqueous CH_3CN, under identical conditions compound **3** has been observed to be insensitive to all the metal ions examined.

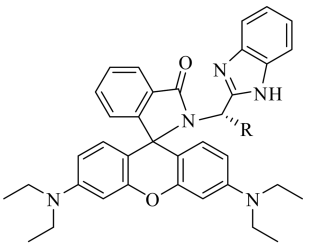

1. R = $C(CH_3)_2$
2. R = Ph
3. R = H

In cation recognition, among various metal ions aluminum is biologically relevant. It is the third most abundant element

Received: April 1, 2017

DOI: 10.1021/acs.inorgchem.7b00835
Inorg. Chem. XXXX, XXX, XXX−XXX

Scheme 1[a]

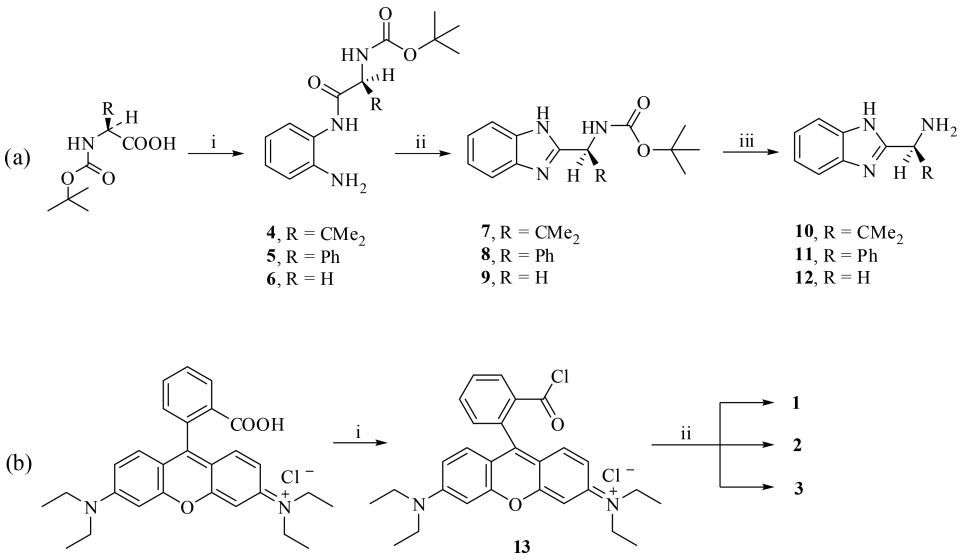

[a]Legend: (a) (i) *o*-phenylenediamine, DCC, dry CH_2Cl_2, 19 h, (ii) AcOH, 80-90 °C, 2 h; (iii) 50% TFA in CH_2Cl_2, 3 h; (b) (i) $POCl_3$, $ClCH_2CH_2Cl$, reflux, 2 h; (ii) **10**/**11**/**12**, Et_3N, dry CH_2Cl_2, 6 h.

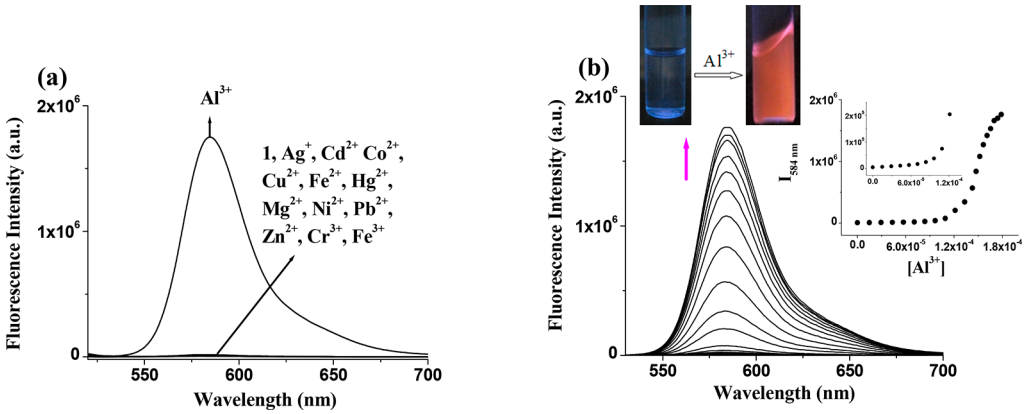

Figure 1. (a) Fluorescence spectra of **1** ($c = 1.5 \times 10^{-5}$ M) with different metal ions (15 equiv) in CH_3CN/H_2O (4/1 v/v; 10 mM tris HCl buffer; pH 7). (b) Fluorescence titration spectra of **1** ($c = 1.5 \times 10^{-5}$ M) in CH_3CN/H_2O (4/1 v/v; 10 mM tris HCl buffer; pH 7) upon addition of Al^{3+} ($c = 1.2 \times 10^{-3}$ M; λ_{exc} 510 nm). Inset: emission intensity of **1** at 584 nm as a function of Al^{3+} concentration and color change of the solution of **1** under illumination of UV light.

(~8% of total mineral components) in the earth's crust.[5] Though aluminum is a nonessential and toxic element for biological systems, our daily life is closely allied with aluminum-based compounds such as in food additives, medicines, cooking utensils, cars, computers etc. Due to the increased solubility of aluminum minerals through acid rain, aluminum toxicity disturbs aquatic life and agricultural production.[6] According to the World Health Organization (WHO), the permissible limit of daily intake of Al^{3+} by humans is about 3−10 mg with a weekly tolerable dietary intake of 7 mg kg^{-1} body weight.[7] Excessive accumulation of Al^{3+} ions in the human body affects neurological systems that may lead to Parkinson's disease, Alzheimer's disease, etc.[8] This ion also acts as a competitive inhibitor for various essential elements such as Mg^{2+}, Ca^{2+}, and Fe^{3+} and affects the metabolism of iron by influencing the absorption of iron via the intestine, hindering iron transport in the serum and displacing iron by binding to transferrin.[9]

The poor coordination and strong hydration ability of Al^{3+} ion in water are some important features that have drawn attention to the development of new classes of compounds for its sensing.[10] A literature survey reveals that rhodamine-coupled architectures for colorimetric detection of Al^{3+} ions are fewer in number in comparison to other cations.[11]

RESULTS AND DISCUSSION

Synthesis. The synthetic pathways of compounds **1**−**3** are outlined in Scheme 1. The *N*-Boc-protected amino acids were transformed into the corresponding benzimidazole amines (**10**−**12**) after performing a series of reactions as mentioned in Scheme 1a. The amines were next reacted with the rhodamine B acid chloride **13** in the presence of Et_3N in dry CH_2Cl_2 to afford the desired compounds **1**−**3** in appreciable yields. All of the compounds were fully characterized by the usual spectroscopic techniques.

Interaction Study. The photophysical properties of the rhodamine-based compounds **1**−**3** were studied by monitoring emission and absorption changes upon addition of various metal ions such as Al^{3+}, Cr^{3+}, Fe^{3+}, Hg^{2+}, Co^{2+}, Pb^{2+}, Fe^{2+}, Cu^{2+}, Ni^{2+}, Mg^{2+}, Zn^{2+}, Cd^{2+}, and Ag^{+} (taken as their perchlorate salts, but for Al^{3+}, $Al_2(SO_4)_3$ was used) in CH_3CN/H_2O

DOI: 10.1021/acs.inorgchem.7b00835
Inorg. Chem. XXXX, XXX, XXX−XXX

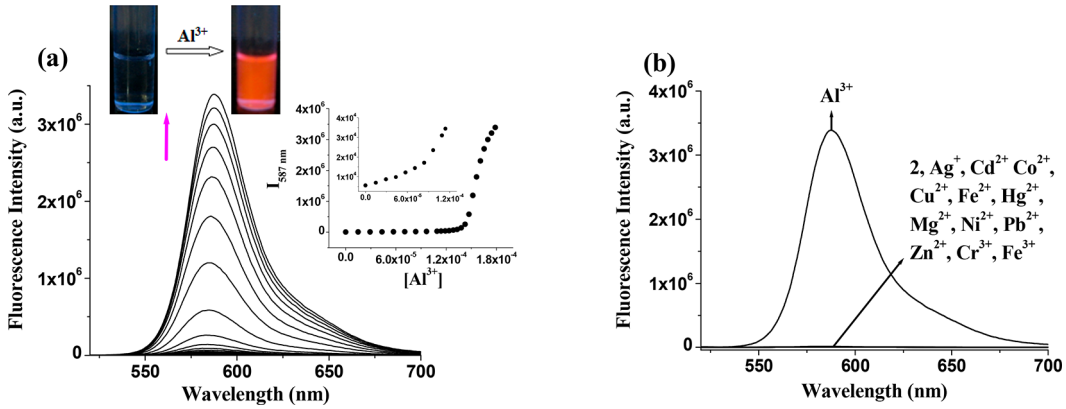

Figure 2. (a) Fluorescence titration spectra of **2** (c = 1.5 × 10^{-5} M) in CH_3CN/H_2O (4/1 v/v; 10 mM tris HCl buffer; pH 7) upon addition of Al^{3+} (c = 1.2 × 10^{-3} M). Inset: emission intensity of **2** at 587 nm as a function of Al^{3+} concentration and color change of the solution of **2** under illumination of UV light. (b) Fluorescence spectra of **2** (c = 1.5 × 10^{-5} M) with different metal ions (15 equiv) in CH_3CN/H_2O (4/1 v/v; 10 mM tris HCl buffer; pH 7) (λ_{exc} 510 nm).

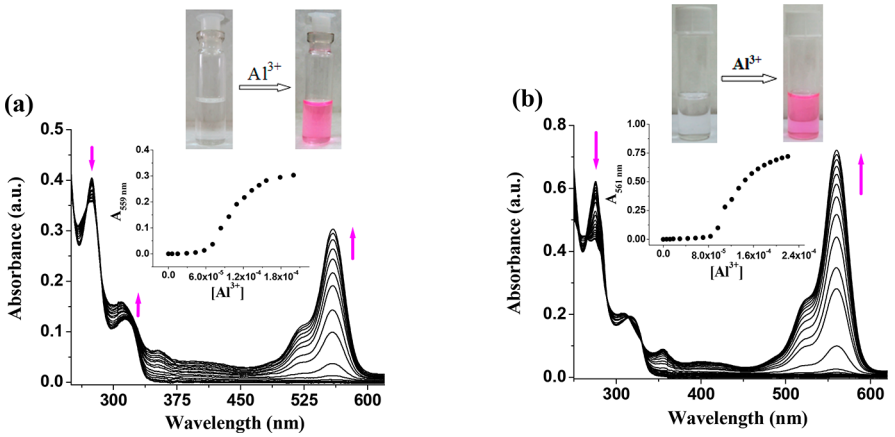

Figure 3. UV−vis titration spectra of (a) **1** (c = 1.5 × 10^{-5} M) and (b) **2** (c = 1.5 × 10^{-5} M) with Al^{3+} (c = 1.2 × 10^{-3} M) ions in CH_3CN/H_2O (4/1 v/v; 10 μM tris HCl buffer; pH 7.0). Inset: absorbance of **1** and **2** at ∼560 nm as a function of Al^{3+} concentration and color changes upon addition of Al^{3+} ions.

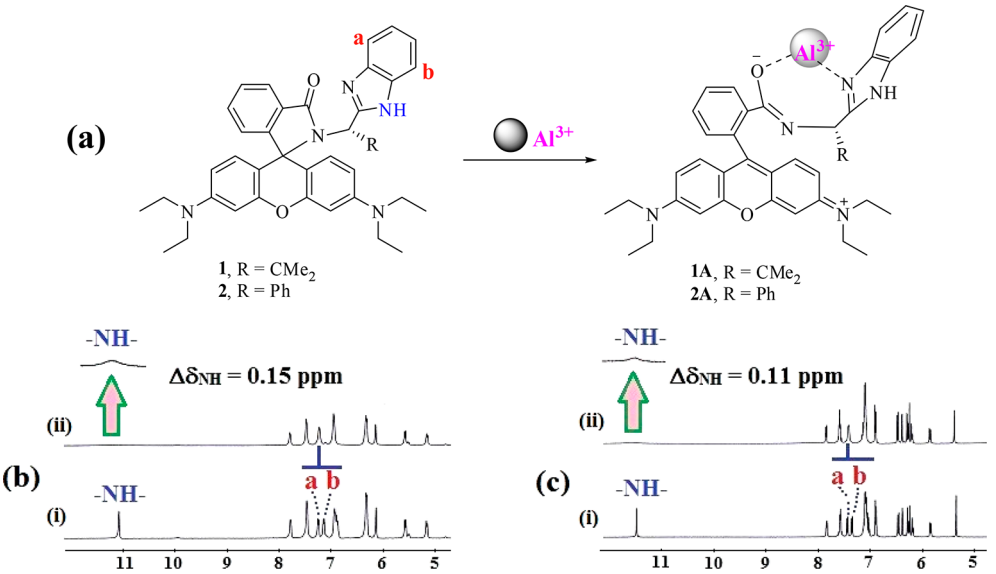

Figure 4. (a) Suggested binding modes of **1** and **2** with Al^{3+} ion and ^{1}H NMR (d_6-DMSO, 400 MHz). Changes of (b) **1** (c = 1.6 × 10^{-2} M) and (c) **2** (c = 1.6 × 10^{-2} M) with 1 equiv of $Al_2(SO_4)_3{\cdot}18H_2O$.

DOI: 10.1021/acs.inorgchem.7b00835
Inorg. Chem. XXXX, XXX, XXX−XXX

(CH_3CN/H_2O 4/1 v/v, 10 mM tris HCl buffer, pH 7). In the absence of metal ions, all three benzimidazole-coupled probes were almost nonfluorescent and colorless. However, upon interaction with only Al^{3+} ions, the L-valine-derived benzimidazole-coupled rhodamine **1** (Φ = 0.011), on excitation at 510 nm, gave a nonstructured emission at 584 nm (Φ = 0.518) with significant intensity and the solution became pink. Other metal ions did not bring any change in emission spectra (Figure 1a and Figure S1 in the Supporting Information). Figure 1b shows the emission titration spectra of **1** with Al^{3+} ions and also the associated color change of the solution under illumination of UV light.

Under identical conditions, compound **2** (Φ = 0.01) was titrated with the same metal ions and, in the study, a fluorescence enhancement (~600-fold) at 587 nm (Φ = 0.642) was observed upon interaction with Al^{3+} ions (Figure 2a) and the solution became pink, like that of **1**. Emission at 587 nm was not observed in the presence of other metal ions examined (Figure 2b and Figure S2 in the Supporting Information). The plots in Figure 1a and Figure 2b, in this regard, clearly show that the probes **1** and **2** are selective to Al^{3+} over other metal ions by exhibiting "turn-on" emission changes.

In a UV–vis study, the change in absorption of **1** upon titration with Al^{3+} was followed. Upon addition of Al^{3+}, a new absorption band centered at 559 nm ($\varepsilon = 2.02 \times 10^4$ M^{-1} cm^{-1}) appeared with increasing intensity and there was a color change from colorless to pink (Figure 3a). The absorption band at 313 nm was increased to a small extent. Other metal ions in the study were silent and did not induce any change in either color or absorption spectra (Figure S3 in the Supporting Information). A similar change in the absorption profile was noticed for **2** on titration with Al^{3+} ions (Figure 3b). The absorption at 275 nm decreased with the appearance of a new absorption at 561 nm ($\varepsilon = 4.8 \times 10^4$ M^{-1} cm^{-1}) upon gradual addition of Al^{3+}. This resulted in an isosbestic point at 313 nm. As for **1**, other metal ions used in the study did not produce such changes in the absorption spectra of **2** (Figure S4 in the Supporting Information).

It should be pointed out that the appearance of a new emission peak at ~585 nm and an absorption peak at ~560 nm for **1** and **2** in the presence of Al^{3+} ions is attributed to the opening of spirolactam rings and generation of the delocalized xanthene moieties, as shown in Figure 4a. In relation to this, the excitation spectra of the aluminum complexes of **1** and **2** (λ_{em} 580 nm) gave good correspondence with their absorption spectra (Figure S5 in the Supporting Information).

To support the proposed binding, we recorded the FTIR and ^1H NMR of both the probes **1** and **2** in the presence and absence of Al salt. The amide carbonyl stretching appearing at 1669 cm^{-1} in **1** was reduced to 1645 cm^{-1} upon complexation of Al^{3+} (Figure S6 in the Supporting Information). Similarly, the carbonyl stretching appearing at 1685 cm^{-1} in **2** moved to 1654 cm^{-1} in the presence of Al^{3+} (Figure S6). Such significant reduction in carbonyl stretching in both cases substantiated the lactam ring opening in the interaction process. In addition, the C=N stretching for benzimidazoles in **1** and **2** which appeared at 1616 and 1615 cm^{-1}, respectively, underwent a blue shift and merged with the amide carbonyl stretching frequencies. The blue shift essentially reflects the strengthening of the C=N bond in the presence of Al^{3+}, and it is ascribed to the inhibition of electronic delocalization around the benzimidazolic unit.[12] In ^1H NMR of **1** in d_6-DMSO, we further note that the signal at 11.07 ppm for benzimidazole NH moves downfield by 0.15 ppm upon complexation with an equivalent amount of Al^{3+}. The signals at 7.23 and 7.13 ppm for the protons of types a and b (see labeling in Figure 4a) merge together at 7.22 ppm during complexation (Figure 4b). A similar pattern was also observed for the probe **2**. The signal for benzimidazole NH at 11.48 ppm also underwent a downfield chemical shift by 0.11 ppm. The overlapping of the signals at 7.43 and 7.34 ppm for the protons of types a and b was observed as for **1** (Figure 4c). These observations in ^1H NMR altogether reveal that the benzimidazole –NHs in **1** and **2** remain intact during interaction with Al^{3+} and follow the binding mode shown in Figure 4a.

Interestingly, when we move to compound **3** (Φ = 0.016) with an aim to understand the interaction with the same metal ions under similar conditions, no measurable change in either absorption or emission spectra (Figure S7 in the Supporting Information) was observed except for Al^{3+}. In fluorescence, on excitation at 510 nm, a small fluorescence enhancement (~7-fold) at ~580 nm (Φ = 0.066) was observed after addition of greater amounts of Al^{3+} ions (50 equiv) and the colorless solution of the probe remained colorless (Figure S8a in the Supporting Information).

In the UV–vis spectrum, a very low intense absorption band at ~560 nm ($\varepsilon = 3.26 \times 10^3$ M^{-1} cm^{-1}) was found in the presence of greater amounts of Al^{3+} ion, but the probe solution was colorless. Figure S8b in the Supporting Information represents the UV–vis titration spectrum of **3** with Al^{3+} ions. Thus, the probe **3** failed to exhibit any appreciable "turn-on" response to Al^{3+} ions, which clearly indicated that the spiro ring remained intact during the interaction.

The differential sensing behaviors of the three compounds are understandable from the plots of fluorescence ratios in Figure 5.

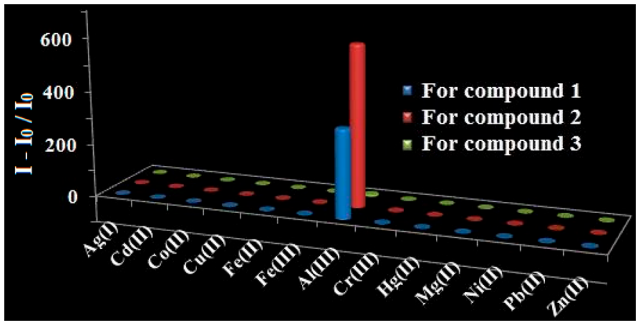

Figure 5. Fluorescence ratios ($(I - I_0)/I_0$) of compounds **1**–**3** ($c = 1.5 \times 10^{-5}$ M) in CH_3CN/water (4/1 v/v; 10 mM tris HCl buffer, pH 7) at 584 nm.

The inertness of **3** toward metal ion sensing in contrast to structures **1** and **2** is interesting. In our opinion, this is associated with the substitutions at the α-positions of the benzimidazoles that presumably influence the orientation of the spirolactam rings with the benzimidazoles and xanthene nucleus and regulate the ring opening differently toward binding of metal ion. To understand this, we tried to grow single crystals of the three compounds. Only single crystals of **2** and **3** were obtained from CH_3OH (Figure 6). For compound **2**, we observe in the solid state the formation of an intramolecular hydrogen bond between the C=O group and the N–H unit from the benzimidazole derivate (N2–H1A···O2 2.205 Å, angle N2–H1A–O2 134.9°; see Figure 6a). The

DOI: 10.1021/acs.inorgchem.7b00835
Inorg. Chem. XXXX, XXX, XXX–XXX

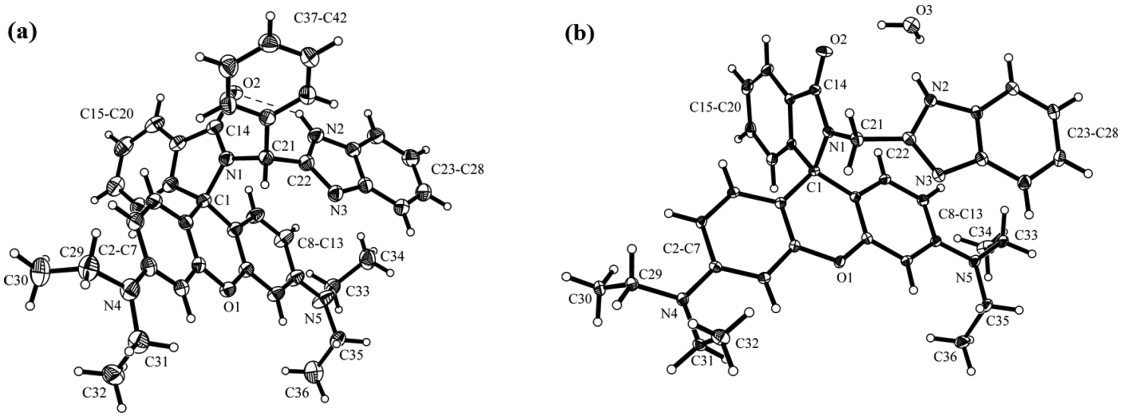

Figure 6. Crystal structures of compounds (a) **2** and (b) **3**. Thermal ellipsoids are shown at 30% probability.

packing diagram of **2** presents the formation of linear chains along the *a* axis involving weak C−H···O and C−H···N intermolecular interactions (see Figure S9a in the Supporting Information; C41−H41···O2B 2.649 Å, angle C41−H41−O2B 157.2°; C35−H35A···N3A 2.692 Å, angle C35−H35A-N3A 128.6°). The $\pi-\pi$ distance between the phenyl rings is about 3.6 Å, which corroborates a weak stacking interaction.

In contrast, the solid state of compound **3** presents no relevant intramolecular interaction between the C═O and N−H units. The distance is longer by about 0.5 Å (N2−H1A···O2 2.734 Å, angle N2−H1A-O2 130.7°). This difference can be explained by the presence of one water molecule found in the crystal structure. Intermolecular interactions between the water molecule and the benzimidazole derivate were found in the solid state (N2−H1A···O3 2.110 Å, angle N2−H1A-O3 150.0°; O3−H2A···N3 2.060 Å, angle O3−H2A-N3 170.0°). These interactions are building spiral chains along the *b* axis (see Figure S9b in the Supporting Information). No other major structural differences were found in the solid state of these two compounds, which can explain the different opening processes of the spirolactam ring. The angles between the planes of benzimidazole and xanthene groups are 14.2° in **3** and 19.8° for compound **2** with a bulky phenyl group. For more information, a theoretical study (see below) was performed.

The selectivity in sensing of Al^{3+} ion by the structure **1** was established by recording the emission of **1** upon adding 15 equiv amounts of Al^{3+} in the presence and absence of 15 equiv amounts of other metal ions. The selectivity plot indicates that the background metal ions have no interference in the binding of Al^{3+} with **1** (Figure S10a in the Supporting Information). Similarly, for structure **2**, the pronounced "off−on" type of Al^{3+} selectivity was also observed even in the presence of other metal ions (Figure S10b). The preferential binding of a particular metal ion into the binding site of a receptor structure depends on various factors such as the nature of coordinating atoms, size of the metal ion, differential solvations, softness/hardness, polarity of solvents, etc.[13] Thus, while the benzimidazole motif in some reported receptor structures[12b,14] is prone to bind metal ions other than aluminum, the selective sensing of Al^{3+} ion over other metal ions in the present study is likely to be due to the change in coordination environment, the polarity of the working solvent that modifies the basicity of the donor atoms involved in binding.

It is notable that chemosensors **1** and **2** both gave the same results in absorption and emission titrations with $Al(NO_3)_3$, $Al(ClO_4)_3{\cdot}9H_2O$, $AlCl_3$, and $K_2SO_4{\cdot}Al_2(SO_4)_3{\cdot}24H_2O$ under similar conditions and thereby ruled out the possibility of any role of the anionic part of the aluminum salts in the sensing process (Figure S11 in the Supporting Information). Moreover, the time course of the fluorescence responses of **1** and **2** upon addition of Al^{3+} was tested. The initial weak fluorescence at 580 nm of sensors **1** and **2** in the metal-free state was stable with time. However, the fluorescence responses of **1** and **2** as tested in the presence of Al^{3+} ions indicate that the reaction of the chemosensors with Al^{3+} ions was rapid and complete within 4 min, after which the fluorescence intensity hardly changed (Figure S12 in the Supporting Information). Thus, the chemosensors are useful in real-time detection of Al^{3+} ions.

In the interactions, the stoichiometries[15] of complexation of the probes **1** and **2** with Al^{3+} ions were evaluated to be 1:1 (Figure S13 in the Supporting Information). The binding constant values of **1** and **2** with Al^{3+} ions as determined by nonlinear[16] fitting of the fluorescence titration data were found to be $(7.71 \pm 0.15) \times 10^3$ and $(6.99 \pm 0.14) \times 10^3$ M^{-1}, respectively (Figure S14 in the Supporting Information). Due to a poor change in emission titrations, we were unable to determine the binding constant values for other metal ions. Analysis of the fluorescence titration data of **1** and **2** with Al^{3+} ions gave detection limits[17] of 6.73×10^{-7} and 8.57×10^{-7} M, respectively (Figure S15 in the Supporting Information).

The effects of pH on emission and as well as on absorption of probes **1**−**3** with and without Al^{3+} ions were also investigated to evaluate the practical applicability of the probes (Figure S16 in the Supporting Information). The results show that probes **1** and **2** were nonfluorescent in the pH range 5−12 but below this range both were highly fluorescent and pink, demonstrating that the spirolactam rings of these two probes were not stable in acidic pH. After addition of Al^{3+} ions to solutions of **1** and **2** under different pH conditions, dramatic enhancement in emission as well as absorption was found from pH 2 to 8 and the colorless solutions became pink (Figure S17A,B in the Supporting Information). In comparison, the probe **3** was almost nonfluorescent and colorless in the wide range of pHs 3−12 (Figure S16). Only at pH 2 slight changes in absorption as well as in emission were observed and indicated that the spiro ring of **3** remained intact at acidic pH. Upon addition of Al^{3+} to the different pH solutions of **3**, no change in absorption and emission as that for **1** and **2** was found and the colorless solution of **3** remained colorless (Figure S17C). This, in addition, pointed out that the spirocyclic ring opening in **3** did not take place even in the presence of Al^{3+} ion.

DOI: 10.1021/acs.inorgchem.7b00835
Inorg. Chem. XXXX, XXX, XXX−XXX

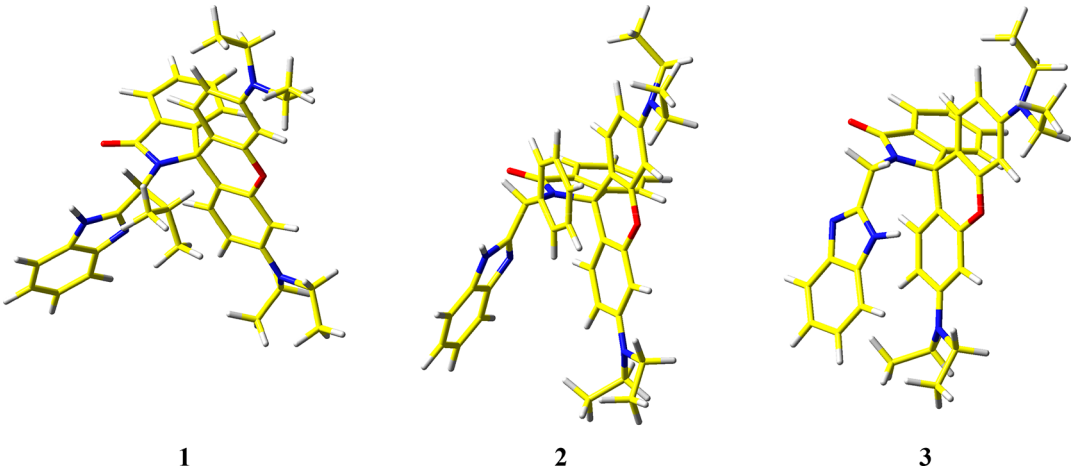

Figure 7. M06-2X/6-31G(d) calculated optimized structures of compounds **1**−**3**.

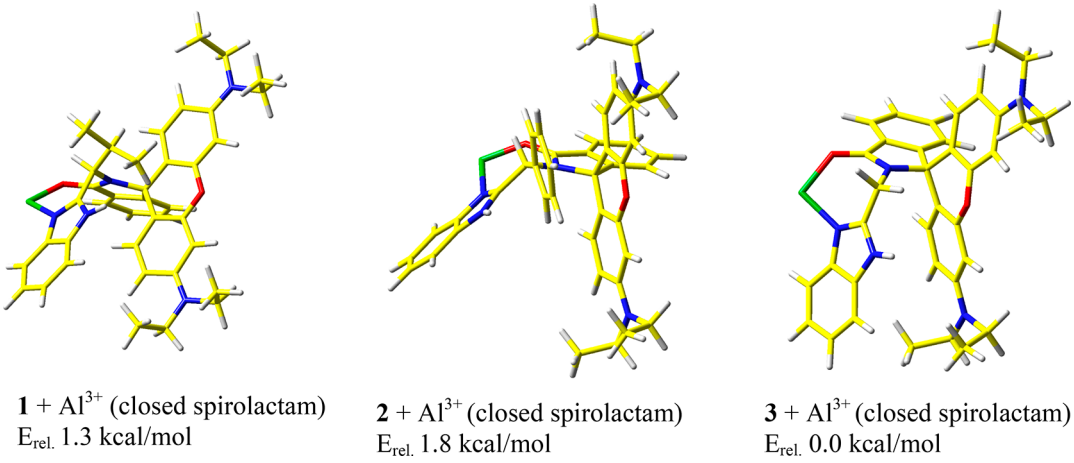

Figure 8. M06-2X/6-31G(d) calculated relative electronic energies (E_{rel}) of compounds **1**−**3** interacting with Al^{3+} in acetonitrile medium when their spirolactam rings are closed. All distances are given in angstroms. Color scheme of atoms: yellow, C; white, H; blue, N; red, O; green, Al.

The reversibility in complexation was realized from recording of emission and absorption spectra of the ensembles of **1** and **2** with Al^{3+} in aqueous CH_3CN by adding different halides. Addition of Cl^-, Br^-, and I^- ions to the ensembles of **1**-Al^{3+} and **2**-Al^{3+} did not bring the reverse changes in both emission and absorption spectra (Figure S18 and S19 in the Supporting Information). Only in the presence of F^- was the pink color of Al complexes was discharged and produced reverse changes in absorption and emission profiles (Figures S18 and S19). The complete decomplexation of Al^{3+} from **1**-Al^{3+} and **2**-Al^{3+} ensembles is ascribed to the high affinity of F^- ions toward Al^{3+} for which in the absence of Al^{3+} the spiro rings are regenerated.

Computational Study. We have carried out DFT (M06-2X) calculations of compounds **1**−**3** in CH_3CN medium at the molecular level (Figure 7) to understand the nature of complexation with Al^{3+}.

First, we computed the complexation energies of Al^{3+} with compounds **1**−**3** having a closed spirolactam ring. The M06-2X/6-31G(d) calculated results show that Al^{3+} forms a relatively more stable complex with compound **3** in comparison to compounds **1** and **2** (Figure 8). The stability of **3** with Al^{3+} ion in comparison to **1** and **2** suggests that the spirolactam ring opening would be less preferred for the former compound.

This study was further extended with DFT calculations to examine the stability of compounds **1**−**3** in an opened spirolactam ring with the presumption that such ring opening would occur with Al^{3+}. The relative complexation energies of Al^{3+} with opened spirolactam-**1** and -**2** are −13.1 and −3.7 kcal/mol, respectively, which are energetically preferred over the opened spirolactam-**3** with Al^{3+} complex (Figure 9). These results corroborate the experimental finding of the ring opening of **1** and **2** easily in the presence of Al^{3+}.

Biological Studies of 1 and 2 in the Presence of Al^{3+}. Due to favorable binding properties of **1** and **2** with Al^{3+} and intense emission in the visible region, it was conceived that both compounds could be exploited for fluorescence imaging of human lung carcinoma cell line A549, particularly for sensitive detection of intracellular Al^{3+} (Figure 10). Hence, to assess the effectiveness of compounds **1** and **2** as probes for intracellular detection of Al^{3+} by fluorescence microscopy, stocks of 2.088 and 1.768 M were prepared in acetonitrile for probes **1** and **2**, respectively. A subsequent substock solution of 1 mM was prepared for both probes in 1X PBS, from which the compounds were added in cell suspensions. Cells were trypsinized and then centrifuged at 300*g* for 15 min. Cell pellets were collected and then washed with 1X PBS. Then cells were incubated with 20 μM of compounds with and without 40 μM $Al(ClO_4)_3$ at 37 °C for 1 h. A drop of the cell suspension

DOI: 10.1021/acs.inorgchem.7b00835
Inorg. Chem. XXXX, XXX, XXX−XXX

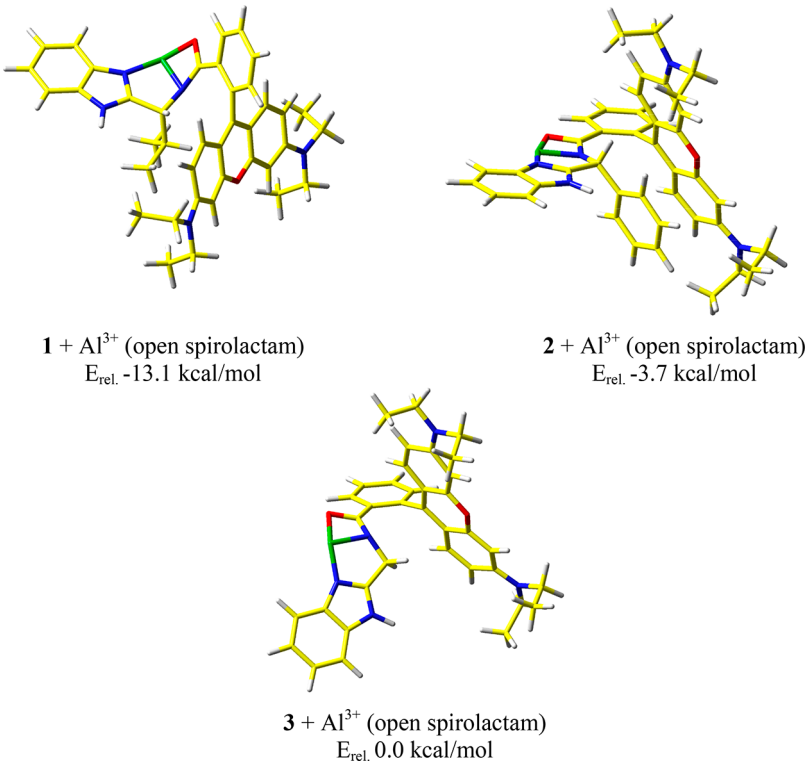

Figure 9. M06-2X/6-31G(d) calculated relative electronic energies (E_{rel}) of compounds **1**−**3** interacting with Al^{3+} in acetonitrile medium when their spirolactam rings are opened. All distances are given in angstroms. Color scheme of atoms: yellow, C; white, H; blue, N; red, O; green, Al.

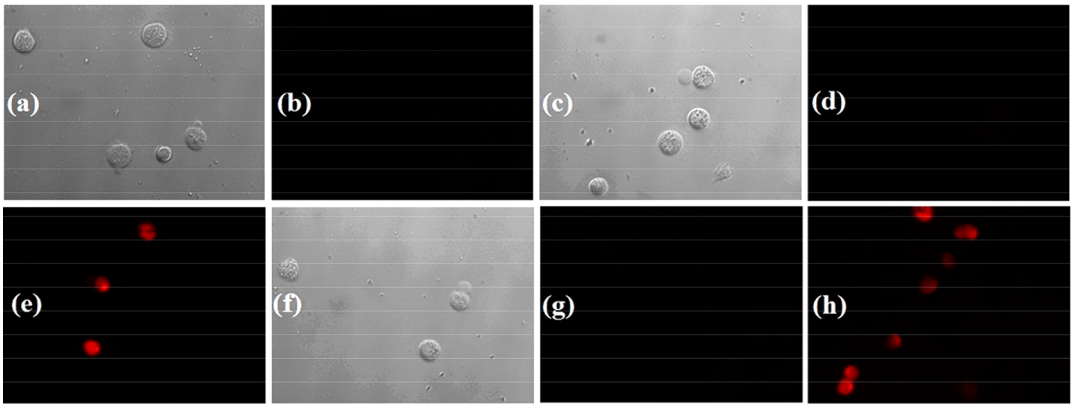

Figure 10. Fluorescence and bright field images of lung cancer cells (A549 cells): (a) bright field image of normal cells; (b) fluorescence image of normal cells; (c) bright field image of cells treated with probe **1** (20 μM) for 1 h at 37 °C; (d) fluorescence image of cells treated with probe **1** (20 μM) for 1 h at 37 °C; (e) fluorescence image of cells upon treatment with probe **1** (20 μM) and then with $Al(ClO_4)_3$ (40 μM) for 1 h at 37 °C; (f) bright field image of cells treated with probe **2** (20 μM) for 1 h at 37 °C; (g) fluorescence image of cells treated with probe **2** (20 μM) for 1 h at 37 °C; (h) fluorescence image of cells upon treatment with probe **2** (20 μM) and then with $Al(ClO_4)_3$ (40 μM) for 1 h at 37 °C.

was mounted over a microscopic slide and observed under the 40× objective of an Axio Scope A1 microscope (Carl Zeiss) for both bright field and fluorescence images. Filter Set 43 with excitation range ∼530−560 nm was used. It is evident from the figure that untreated normal cells do not have any fluorescence, as shown in Figure 10b. Treatment of cells with probes **1** and **2** separately did not show fluorescence from cells (Figure 10d,g). However, when the probe-treated cells in each case were incubated with $Al(ClO_4)_3$, they fluoresced red when filter set 43 filter was used (Figures 10e,h). This fluorescence microscopic analysis strongly suggested that compounds **1** and **2** could readily cross the membrane barrier, permeate into cells, and rapidly sense intracellular Al^{3+}. Further, to verify the cell viability in the presence of compounds **1** and **2**, a conventional MTT assay was performed. In the study, A549 cells were seeded in 96-well plates in triplicate manner (Figure S20 in the Supporting Information). Cells were incubated with 20, 25, and 30 μM compounds for 4 h. It is evident from the result that compounds **1** and **2** both have very little effect on cell viability.

CONCLUSION

In summary, we have designed and synthesized some α-amino acid derived benzimdazole-linked rhodamine compounds **1**−**3** with different substituents on the amino acid part. Among the structures, only compounds **1** and **2** bind and sense Al^{3+} ion selectively over the other ions studied by exhibiting "turn-on"

DOI: 10.1021/acs.inorgchem.7b00835
Inorg. Chem. XXXX, XXX, XXX−XXX

response in electronic and fluorescence spectra in the visible region. The selectivity, binding constant values, and detection limits are praiseworthy and are comparable with the reported structures of various architectures (Table S2 in the Supporting Information). However, the response of the compounds depends on the nature of the α-substitutions of the amino acid motifs. Experimental results reveal that the rhodamine–benzimidazole conjugate without α-substitution at the amino acid motif (compound **3** in the present case) is evaluated to be stable to metal ions and acid as well. The substitutions at the α-positions of the benzimidazoles presumably influence the orientation of the spirolactam rings with the benzimidazoles and xanthene nucleus and regulate the ring opening differently toward binding of metal ion. The crystal structure analysis and theoretical insight explain the reactivity profiles. As compounds **1** and **2** work under physiological conditions, both compounds are preferred for use either as colorimetric staining agents or as reagents for imaging studies with biological and environmental samples. In practice, both **1** and **2**, when applied in human lung carcinoma cell line A549, could detect successfully the cellular uptake of Al^{3+} ion.

EXPERIMENTAL SECTION

(*S*)-*tert*-Butyl 1-(2-Aminophenylamino)-3-methyl-1-oxobutan-2-ylcarbamate[18] (4). To a stirred solution of *N*-Boc-protected L-valine acid (1 g, 4.6 mmol) in dry CH_2Cl_2 (15 mL) was added DCC (1 g, 4.84 mmol) at 0 °C. The solution was stirred for 30 min, and a solution of *o*-phenylenediamine (2.5 g, 23.11 mmol) in dry CH_2Cl_2 (35 mL) was added to it under a nitrogen atmosphere. After it was stirred for 19 h, the reaction mixture was filtered off to remove insoluble DCU. The filtrate was removed in vacuo, and the crude product was purified by silica gel column chromatography using 1% CH_3OH in $CHCl_3$ to afford compound **4** (0.92 g, yield 65%): mp 132 °C; ^{1}H NMR (400 MHz, $CDCl_3$) δ 7.75 (s, 1H), 7.21 (d, 1H, J = 8 Hz), 7.05 (t, 1H, J = 8 Hz), 6.79–6.75 (m, 2H), 5.12 (br s, 1H), 3.99 (t, 1H, J = 8 Hz), 3.87 (s, 2H), 2.29–2.25 (m, 1H), 1.65 (s, 9H), 1.12–1.01 (m, 6H); FT-IR ν cm^{-1} (KBr) 3420, 3339, 3257, 3044, 2980, 1703, 1678, 1538.

(*S*)-*tert*-Butyl 2-(2-Aminophenylamino)-2-oxo-1-phenylethylcarbamate (5). Using the same strategy as for compound **4**, we synthesized compound **5** (yield 68%); mp 138 °C; ^{1}H NMR (400 MHz, $CDCl_3$) δ 7.78 (s, 1H), 7.44 (d, 2H, J = 8 Hz), 7.38–7.32 (m, 3H), 7.11 (d, 1H, J = 8 Hz), 7.01 (t, 1H, J = 8 Hz), 6.74–6.69 (m, 2H), 5.87 (d, 1H, J = 4 Hz), 5.36 (s, 1H), 3.65 (s, 2H), 1.42 (s, 9H); FT-IR ν cm^{-1} (KBr) 3347, 3257, 2977, 1708, 1661, 1523, 1456.

(*S*)-*tert*-butyl 1-(1*H*-benzo[*d*]imidazol-2-yl)-2-methylpropylcarbamate[18] (7). Compound **4** (0.5 g, 1.63 mmol) was next heated in acetic acid (0.5 mL) at 80 °C for 2 h. Then the reaction mixture was quenched by addition of an aqueous solution of $NaHCO_3$ (15 mL). The reaction mixture was next extracted with a $CHCl_3$/MeOH solvent mixture ($CHCl_3$/MeOH 3/1 v/v; 20 mL). The organic layer was washed with brine, dried over Na_2SO_4, and evaporated under reduced pressure. The reaction mixture was purified by silica gel column chromatography using 40% petroleum ether in ethyl acetate to afford the compound **7** (0.415 g, yield 88%): mp 174 °C; ^{1}H NMR (400 MHz, $CDCl_3$ containing one drop of d_6-DMSO) δ 10.70 (s, 1H), 7.71 (d, 1H, J = 8 Hz), 7.35 (d, 1H, J = 8 Hz), 7.21–7.19 (m, 2H), 5.67 (d, 1H, J = 8 Hz), 4.61 (t, 1H, J = 8 Hz), 2.47–2.45 (m, 1H), 1.43 (s, 9H), 1.06 (d, 3H, J = 4 Hz), 0.93 (d, 3H, J = 4 Hz); ^{13}C NMR (100 MHz, $CDCl_3$ containing one drop of d_6-DMSO) δ 155.6, 154.9, 121.7 (four carbons unresolved), 79.2, 55.1, 33.2, 28.2, 19.2, 18.3; FT-IR ν cm^{-1} (KBr) 3333, 2974, 2930, 1675, 1628, 1536.

(*S*)-*tert*-Butyl (1*H*-Benzo[*d*]imidazol-2-yl)(phenyl)methylcarbamate (8). Using the strategy followed for compound **7**, compound **8** was prepared in 85% yield: mp 190 °C; ^{1}H NMR (400 MHz, $CDCl_3$) δ 10.15 (s, 1H), 7.71 (d, 1H, J = 8 Hz), 7.36 (m, 2H), 7.35–7.29 (m, 2H), 7.27–7.25 (m, 2H), 7.24–7.19 (m, 2H), 6.24 (brs, 1H), 6.09 (s, 1H), 1.42 (s, 9H); FT-IR ν cm^{-1} (KBr) 3329, 2935, 1673, 1528, 1454, 1442.

***tert*-Butyl (1*H*-Benzo[*d*]imidazol-2-yl)methylcarbamate[19] (9).** Using the strategy followed for compound **7**, compound **9** was prepared in 88% yield: mp 174 °C; ^{1}H NMR (400 MHz, $CDCl_3$) δ 10.30 (s, 1H), 7.70 (br s, 1H), 7.52 (br s, 1H), 7.25–7.23 (m, 2H), 5.55 (br t, 1H), 4.51 (d, 2H, J = 8 Hz), 1.30 (s, 9H); FT-IR ν cm^{-1} (KBr) 3348, 2978, 2931, 2751, 1688, 1529.

Compound 1. To synthesize compound **1**, a solution of rhodamine B (0.1 g, 0.2 mmol) in 1,2-dichloroethane (10 mL) was stirred and phosphorus oxychloride (250 μL) was added dropwise at room temperature. Then the resulting solution was refluxed for 2 h. The reaction mixture was cooled and evaporated in vacuo to give rhodamine B acid chloride **13**, which was used in the next step directly. The acid chloride was dissolved in dry dichloromethane (10 mL) and was added dropwise over 10 min to a solution of amine **10** (0.06 g, 0.317 mmol; obtained from deprotection of Boc-group in **7** using TFA) and Et_3N (70 μL) in dichloromethane (10 mL) at room temperature and stirred for 8 h. After completion of the reaction as monitored by TLC, the solvent was removed under pressure and the residue was dissolved in chloroform, extracted with water, and dried over anhydrous Na_2SO_4. The crude mass was purified by silica gel column chromatography using petroleum ether/ethyl acetate (7/3 v/v) as eluent, giving a white powder of compound **1** (0.09 g, yield 70%): mp 96 °C; $[\alpha]_D^{25} = -112.13$ (c = 0.305 g/100 mL in $CHCl_3$); ^{1}H NMR (400 MHz, $CDCl_3$) δ 10.44 (s, 1H), 7.94 (m, 1H), 7.49 (t, 2H, J = 8 Hz), 7.33 (brm, 2H), 7.14 (t, 1H, J = 4 Hz), 7.07 (brm, 2H), 6.55 (d, 1H, J = 8 Hz), 6.43 (d, 1H, J = 4 Hz), 6.38 (d, 1H, J = 8 Hz), 6.33 (d, 1H, J = 8 Hz), 5.64 (d, 1H, J = 8 Hz), 5.25 (d, 1H, J = 8 Hz), 3.82 (d, 1H, J = 10.8 Hz), 3.39–3.34 (m, 4H), 3.20–3.09 (m, 2H), 3.01–2.94 (m, 2H), 1.72 (brs, 1H), 1.18 (t, 6H, J = 7.20 Hz), 0.95 (t, 6H, J = 7.20 Hz), 0.62 (t, 6H, J = 7.20 Hz); ^{13}C NMR (100 MHz, $CDCl_3$) δ 168.2, 153.6, 153.2, 152.4, 151.5, 148.1, 147.5, 131.8, 131.1, 129.4, 127.2, 125.9, 123.2, 121.5, 120.5, 106.6, 106.4, 103.3, 103.0, 97.02, 96.6, 66.4, 59.4, 43.4, 43.0, 28.4, 19.8, 19.0, 11.56, 11.53; FT-IR ν cm^{-1} (KBr) 3333, 2965, 2928, 1669, 1634, 1616, 1515; HRMS (TOF MS ES$^+$) calcd for $(M + H)^+$ 614.3495, found 614.3495.

Compound 2. According to the procedure as followed for the synthesis of **1**, compound **2** was prepared (0.092 g, yield 68%); mp 216 °C; $[\alpha]_D^{25} = -0.8$ (c = 0.6 g/100 mL in CH_3OH); ^{1}H NMR (400 MHz, d_6-DMSO) δ 11.48 (s, 1H), 7.82 (d, 1H, J = 8 Hz), 7.57–7.55 (m, 2H), 7.43 (d, 1H, J = 8 Hz), 7.34 (d, 1H, J = 8 Hz), 7.11–7.02 (m, 6H), 6.88 (d, 2H, J = 4 Hz), 6.45 (d, 1H, J = 8 Hz), 6.38 (s, 1H), 6.28–6.19 (m, 3H), 5.85 (d, 1H, J = 8 Hz), 5.34 (s, 1H), 3.50–3.30 (m, 4H, buried under signal of solvent), 3.16- 3.11 (m, 4H), 1.09 (t, 6H, J = 8 Hz), 0.91 (t, 6H, J = 8 Hz); ^{13}C NMR (100 MHz, d_6-DMSO) δ 166.9, 153.4, 153.3, 153.0, 152.5, 148.8, 148.6, 142.9, 138.4, 134.8, 133.5, 131.7, 129.8, 129.5, 128.8, 128.6, 128.0, 127.3, 124.3, 122.9, 122.1, 121.2, 118.7, 112.1, 108.5, 107.9, 104.8, 104.1, 97.4, 66.4, 56.2, 44.2, 44.0, 12.8, 12.7; FT-IR ν cm^{-1} (KBr) 3293, 2966, 1685, 1635, 1615, 1545, 1514; HRMS (TOF MS ES$^+$): C calcd for $(M + H)^+$ 648.3339, found 648.3364.

Compound 3. According to the procedure followed for the synthesis of **1**, compound **3** was prepared (0.12 g, yield 67%): mp 160 °C; ^{1}H NMR (400 MHz, $CDCl_3$) δ 9.90 (s, 1H), 7.96–7.94 (m, 1H), 7.48–7.44 (m, 3H), 7.26 (s, 1H), 7.14–7.07 (m, 3H), 6.37 (d, 2H, J = 2.4 Hz), 6.22 (s, 1H), 6.20 (s, 1H), 5.94 (dd, 2H, J_1 = 8 Hz, J_2 = 4 Hz), 4.56 (s, 2H), 3.27–3.17 (m, 8H), 1.08 (t, 12H, J = 8 Hz); ^{13}C NMR (100 MHz, $CDCl_3$) δ 169.2, 153.6, 153.4, 150.8, 148.8, 133.0, 130.3, 128.2, 128.0, 124.0, 122.8, 121.9, 108.4, 107.8, 103.9, 97.8, 65.8, 44.2, 38.2, 12.5; FT-IR ν cm^{-1} (KBr) 3512, 2970, 1693, 1680, 1634, 1615, 1547, 1515; HRMS (TOF MS ES$^+$) calcd for $(M + H)^+$ 572.3026, found 572.3018.

Quantum Yield Determination. Quantum yields (Φ) of the compounds **1**–**3** by themselves and in the presence of Al^{3+} were determined in CH_3CN by a relative comparison procedure using rhodamine B as standard ($\Phi_{rh\,6G}$ = 0.95 in ethanol).[20a] The general equation used for determination of relative quantum yields is[20b]

$$\Phi_u = (\Phi_s F_u A_s \lambda_{exs} \eta^2_u)/(F_s A_u \lambda_{exu} \eta^2_s)$$

DOI: 10.1021/acs.inorgchem.7b00835
Inorg. Chem. XXXX, XXX, XXX–XXX

where Φ is the quantum yield, F is the integrated area under the corrected emission spectrum, A is the absorbance at the excitation wavelength, λ_{ex} is the excitation wavelength, η is the refractive index of the solution, and the subscripts u and s refer to the unknown and the standard, respectively.

X-ray Diffraction. Data sets for compound **2** were collected with a Nonius Kappa CCD diffractometer. Programs used: data collection, COLLECT;[21] data reduction, DENZO-SMN;[22] absorption correction, DENZO.[23] For compound **3** data sets were collected with a D8 Venture Dual Source 100 CMOS diffractometer. Programs used: data collection, APEX3;[24] cell refinement and data reduction, SAINT;[24] absorption correction, SADABS;[24] structure solution and structure refinement, SHELXL[25] and SHELXTL;[26] and graphics, XP.[27] R1 values are given for observed reflections, and wR2 values are given for all reflections.

Exceptions and Special Features. For compound **2** the hydrogen atom positions at the N2 atom were refined freely. Two isopropyl groups were found to be disordered over two positions. Several restraints (SADI, SAME, ISOR, and SIMU) were used in order to improve refinement stability. Compound **3** crystallizes by chance in the Sohncke space group $P2_1$ and was refined as a two-component inversion twin (with BASF 0.20). The hydrogen atom positions at N2 and O3 atoms were refined freely.

X-ray Crystal Structure Analysis of ***2****.* Crystal data are as follows: formula $C_{42}H_{41}N_5O_2$, M_r = 647.80, colorless crystal, 0.22 × 0.18 × 0.02 mm, a = 16.7855(3) Å, b = 9.6854(2) Å, c = 22.4428(5) Å, β = 111.048(1)°, V = 3405.2(1) Å^3, ρ_{calc} = 1.264 g cm^{-3}, μ = 0.079 mm^{-1}, empirical absorption correction ($0.982 \leq T \leq 0.998$), Z = 4, monoclinic, space group $P2_1/c$ (No. 14), λ = 0.71073 Å, T = 223(2) K, ω and φ scans, 25844 reflections collected ($\pm h$, $\pm k$, $\pm l$), 8349 independent (R_{int} = 0.067) and 5459 observed reflections ($I > 2\sigma(I)$), 486 refined parameters, R1 = 0.084, wR2 = 0.185, maximum (minimum) residual electron density 0.26 (−0.31) e Å^{-3}, hydrogen atom at N2 refined freely; other atoms calculated and refined as riding atoms.

X-ray Crystal Structure Analysis of ***3****.* A pale yellow prismlike specimen of $C_{36}H_{37}N_5O_2{\cdot}H_2O$, approximate dimensions 0.084 mm × 0.117 mm × 0.177 mm, was used for the X-ray crystallographic analysis. The X-ray intensity data were measured. A total of 1054 frames were collected. The total exposure time was 19.17 h. The frames were integrated with the Bruker SAINT software package using a wide-frame algorithm. The integration of the data using a monoclinic unit cell yielded a total of 19806 reflections to a maximum θ angle of 68.30° (0.83 Å resolution), of which 5650 were independent (average redundancy 3.505, completeness 99.8%, R_{int} = 3.81%, R_{sig} = 3.54%) and 5242 (92.78%) were greater than $2\sigma(F^2)$. The final cell constants of a = 11.8491(3) Å, b = 11.1111(3) Å, c = 11.8732(3) Å, β = 100.1190(10)°, and V = 1538.87(7) Å^3 are based upon the refinement of the XYZ centroids of 9937 reflections above $20\sigma(I)$ with 7.563° < 2θ < 136.3°. Data were corrected for absorption effects using the multiscan method (SADABS). The ratio of minimum to maximum apparent transmission was 0.931. The calculated minimum and maximum transmission coefficients (based on crystal size) are 0.8930 and 0.9470, respectively. The structure was solved and refined using the Bruker SHELXTL Software Package, using the space group $P2_1$, with Z = 2 for the formula unit, $C_{36}H_{37}N_5O_2{\cdot}H_2O$. The final anisotropic full-matrix least-squares refinement on F^2 with 414 variables converged at R1 = 2.94% for the observed data and wR2 = 7.24% for all data. The goodness of fit was 1.053. The largest peak in the final difference electron density synthesis was 0.131 e Å^{-3}, and the largest hole was −0.134 e Å^{-3} with an RMS deviation of 0.029 e Å^{-3}. On the basis of the final model, the calculated density was 1.273 g/cm^3 and F(000) was 628 e.

Computational Details. Full geometrical optimizations have been carried out in the gas phase employing the M06-2X level[28] with the standard 6-31G(d) basis set. The hybrid meta-functional M06-2X has been considered as an excellent DFT functional for considering the noncovalent interactions,[29] and it predicts the accurate valence and Rydberg electronic excitation energies for main-group chemistry.[28a] Frequency calculations were performed at the same level of theory, to confirm that each stationary point is a local minimum (with zero imaginary frequency). Single-point calculations were executed at the same level of theory to account the solvation effects with the polarizable continuum model (PCM) in acetonitrile (ε = 35.688). All calculations have been performed with the Gaussian 09 suite of programs.[30]

■ ASSOCIATED CONTENT

Supporting Information

The Supporting Information is available free of charge on the ACS Publications website at DOI: 10.1021/acs.inorgchem.7b00835.

Fluorescence and UV−vis titrations of compounds **1**−**3** with various metal ions, Job plots, binding constant curves, detection limit plots, and other spectral data (PDF)

Accession Codes

CCDC 1496178−1496179 contain the supplementary crystallographic data for this paper. These data can be obtained free of charge via www.ccdc.cam.ac.uk/data_request/cif, or by emailing data_request@ccdc.cam.ac.uk, or by contacting The Cambridge Crystallographic Data Centre, 12 Union Road, Cambridge CB2 1EZ, UK; fax: +44 1223 336033.

■ AUTHOR INFORMATION

Corresponding Authors

*B.G.: e-mail, ganguly@csmcri.org.

*K.G.: e-mail, ghosh_k2003@yahoo.co.in; fax, +913325828282; tel, +913325828750.

ORCID

Bishwajit Ganguly: 0000-0002-9858-3165

Kumaresh Ghosh: 0000-0003-1236-8139

Notes

The authors declare no competing financial interest.

■ ACKNOWLEDGMENTS

A.M. thanks the CSIR and S.M. thanks the UGC, New Delhi, India, for fellowships. K.G. thanks the DST, West Bengal, India, for financial support (project sanc. No. 755(Sanc.)/ST/P/S&T/4G-3/2014 dated 27.11.2014).

■ REFERENCES

(1) (a) Kim, H. N.; Ren, W. X.; Kim, J. S.; Yoon, J. Fluorescent and colorimetric sensors for detection of lead, cadmium, and mercury ions. *Chem. Soc. Rev.* **2012**, *41*, 3210−3244. (b) Gupta, A.; Kumar, N. A review of mechanisms for fluorescent "turn-on" probes to detect Al^{3+} ions. *RSC Adv.* **2016**, *6*, 106413−10434. (c) Jeong, Y.; Yoon, J. Recent progress on fluorescent chemosensors for metal ions. *Inorg. Chim. Acta* **2012**, *381*, 2−14. (d) Sun, Z.; Cui, G.; Li, H.; Liu, Y.; Tian, Y.; Yan, S. Multifunctional optical sensing probes based on organic−inorganic hybrid composites. *J. Mater. Chem. B* **2016**, *4*, 5194−5216. (e) Peng, Y.; Dong, Y.-M.; Wang, Y.-W. A Selective, Sensitive, Colorimetric, and Fluorescence Probe for Relay Recognition of Fluoride and Cu(II) Ions with "Off−On−Off" Switching in Ethanol-Water Solution. *J. Org. Chem.* **2012**, *77*, 9072−9080.

(2) (a) Quang, D. T.; Kim, J. S. Fluoro- and Chromogenic Chemodosimeters for Heavy Metal Ion Detection in Solution and Biospecimens. *Chem. Rev.* **2010**, *110*, 6280−6301. (b) de Silva, A. P.; Moody, T. S.; Wright, G. D. Fluorescent PET (Photoinduced Electron Transfer) sensors as potent analytical tools. *Analyst* **2009**, *134*, 2385−2393. (c) Gunnlaugsson, T.; Leonard, J. P.; Murray, N. S. Highly Selective Colorimetric Naked-Eye Cu(II) Detection Using an Azobenzene Chemosensor. *Org. Lett.* **2004**, *6*, 1557−1560.

DOI: 10.1021/acs.inorgchem.7b00835
Inorg. Chem. XXXX, XXX, XXX−XXX

(3) (a) Ramette, R. W.; Sandell, E. B. Rhodamine B Equilibria. *J. Am. Chem. Soc.* **1956**, *78*, 4872−4878. (b) Chen, X.; Pradhan, T.; Wang, F.; Kim, J. S.; Yoon, J. Fluorescent Chemosensors Based on Spiroring-Opening of Xanthenes and Related Derivatives. *Chem. Rev.* **2012**, *112*, 1910−1956. (c) Zheng, H.; Zhan, X.-Q.; Bian, Q.-N.; Zhang, X.-J. Advances in modifying fluorescein and rhodamine fluorophores as fluorescent chemosensors. *Chem. Commun.* **2013**, *49*, 429−447. (d) Kumar, N.; Bhalla, V.; Kumar, M. Resonance energy transfer-based fluorescent probes for Hg^{2+}, Cu^{2+} and Fe^{2+}/Fe^{3+} ions. *Analyst* **2014**, *139*, 543−558. (e) Pal, S.; Chatterjee, N.; Bharadwaj, P. K. Selectively sensing first-row transition metal ions through fluorescence enhancement. *RSC Adv.* **2014**, *4*, 26585−26620. (f) Zhang, R.; Yan, F.; Huang, Y.; Kong, D.; Ye, Q.; Xu, J.; Chen, L. Rhodamine-based ratiometric fluorescent probes based on excitation energy transfer mechanisms: construction and applications in ratiometric sensing. *RSC Adv.* **2016**, *6*, 50732−50760. (g) Tang, J.-L.; Li, C.-Y.; Li, Y.-F.; Zho, C.-X. A ratiometric fluorescent probe with unexpected high selectivity for ATP and its application in cell imaging. *Chem. Commun.* **2014**, *50*, 15411−15414. (h) Saha, S.; Mahato, P.; Baidya, M.; Das, A. An interrupted PET coupled TBET process for the design of a specific receptor for Hg^{2+} and its intracellular detection in MCF7 cells. *Chem. Commun.* **2012**, *48*, 9293−9295. (i) Saha, S.; Mahato, P.; Reddy, G.; Suresh, U.; Chakrabarty, E.; Biadya, A.; Ghosh, M.; Das, S. K. A. Recognition of Hg^{2+} and Cr^{3+} in physiological conditions by a rhodamine derivative and its application as reagent for cell imaging studies. *Inorg. Chem.* **2012**, *51*, 336−345. (j) Kim, H. N.; Lee, M. H.; Kim, H. J.; Kim, J. S.; Yoon, J. A new trend in rhodamine-based chemosensors: application of spirolactam ring-opening to sensing ions. *Chem. Soc. Rev.* **2008**, *37*, 1465−1472. (k) Beija, M.; Afonso, C. A. M.; Martinho, J. M. G. Synthesis and applications of Rhodamine derivatives as fluorescent probes. *Chem. Soc. Rev.* **2009**, *38*, 2410−2433. (l) Culzoni, M. J.; de la Peña, A. M.; Machuca, A.; Goicoechea, H. C.; Babiano, R. Rhodamine and BODIPY chemodosimeters and chemosensors for the detection of Hg^{2+}, based on fluorescence enhancement effects. *Anal. Methods* **2013**, *5*, 30−49. (m) Suresh, M.; Shrivastav, M.; Mishra, S.; Suresh, E.; Das, A. A Rhodamine-Based Chemosensor that Works in the Biological System. *Org. Lett.* **2008**, *10*, 3013−3016. (n) Cai, S.; Lu, Y.; He, S.; Wei, F.; Zhao, L.; Zeng, X. A highly sensitive and selective turn-on fluorescent chemosensor for palladium based on a phosphine-rhodamine conjugate. *Chem. Commun.* **2013**, *49*, 822−824. (o) Yang, Y.; Gao, C.-Y.; Liu, J.; Dong, D. Recent developments in rhodamine salicylidene hydrazone chemosensors. *Anal. Methods* **2016**, *8*, 2863−2871. (p) Reddy, G. U.; Anila, H. A.; Ali, F.; Taye, N.; Chattopadhyay, S.; Das, A. FRET-Based Probe for Monitoring pH Changes in Lipid-Dense Region of Hct116 Cells. *Org. Lett.* **2015**, *17*, 5532−5535. (q) Reddy, G. U.; Ramu, V.; Roy, S.; Taye, N.; Chattopadhyay, S.; Das, A. A specific probe for Hg^{2+} to delineate even H^+ in pure aqueous buffer/Hct116 colon cancer cells: Hg(II)−η^2-arene π-interaction and a TBET-based fluorescence response. *Chem. Commun.* **2014**, *50*, 14421−14424. (r) Fang, Y.; Zhou, Y.; Rui, Q.; Yao, C. Rhodamine-Ferrocene conjugate chemosensor for selectively sensing Copper(II) with multisignals: chromaticity, fluorescence, and electrochemistry and its application in living cell imaging. *Organometallics* **2015**, *34*, 2962−2970. (s) Mahato, P.; Saha, S.; Das, P.; Agarwalla, H.; Das, A. An overview of the recent developments on Hg^{2+} recognition. *RSC Adv.* **2014**, *4*, 36140−36174. (t) Huang, J.; Xu, Y.; Qian, X. Rhodamine-based fluorescent off-on sensor for Fe^{3+} - in aqueous solution and in living cells: 8-aminoquinoline receptor and 2:1 binding. *Dalton Trans.* **2014**, *43*, 5983−5989. (u) Reddy, G. U.; Ali, F.; Taye, N.; Chattopadhyay, S.; Das, A. A new turn on Pd^{2+}-specific fluorescence probe and its use as an imaging reagent for cellular uptake in Hct116 cells. *Chem. Commun.* **2015**, *51*, 3649−3652.

(4) (a) Ghosh, K.; Sarkar, A. R.; Samadder, A.; Khuda-Bukhsh, A. R. Pyridinium-Based Fluororeceptors As Practical Chemosensors for Hydrogen Pyrophosphate ($HP_2O_7^{3-}$) in Semiaqueous and Aqueous Environments. *Org. Lett.* **2012**, *14*, 4314−4317. (b) Ghosh, K.; Sarkar, T.; Samadder, A. R. A rhodamine appended tripodal receptor as a ratiometric probe for Hg^{2+} ions. *Org. Biomol. Chem.* **2012**, *10*, 3236−3243. (c) Ghosh, K.; Sarkar, A. R.; Chattopadhyay, A. P. Anthracene-Labeled 1,2,3-Triazole-Linked Bispyridinium Amide for Selective Sensing of $H_2PO_4^-$ by Fluorescence and Gel Formation. *Eur. J. Org. Chem.* **2012**, *2012*, 1311−1317. (d) Ghosh, K.; Kar, D.; Frohlich, R.; Chattopadhyay, A. P.; Samadder, A.; Khuda-Bukhsh, A. R. *O*-tert-Butyldiphenylsilyl coumarin and dicoumarol: a case toward selective sensing of F^- ions in organic and aqueous environments. *Analyst* **2013**, *138*, 3038−3045. (e) Ghosh, K.; Tarafdar, D.; Petsalakis, I. D.; Theodorakopoulos, G. A Pyridinium- Urea- Coupled Polyether Receptor for the Selective Sensing of Lysine and Cell Imaging. *Eur. J. Org. Chem.* **2017**, *2017*, 355−362. (f) Ghosh, K.; Majumdar, A. Isomeric chiral pyrrole diamides and their efficacy in enantioselective sensing of tartrate in sol-gel medium. *Tetrahedron Lett.* **2016**, *57*, 3629−3634.

(5) (a) Miller, W. S.; Zhuang, L.; Bottema, J.; Wittebrood, A. J.; Smet, P. D.; Haszler, A.; Vieregge, A. Recent development in aluminium alloys for the automotive industry. *Mater. Sci. Eng., A* **2000**, *280*, 37−49. (b) Ciardelli, G.; Ranieri, N. The treatment and reuse of waste water in the textile industry by means of ozonation and electroflocculation. *Water Res.* **2001**, *35*, 567−572.

(6) (a) Poleo, A. B. S.; et al. Toxicity of acid aluminium-rich water to seven freshwater fish species: a comparative laboratory study. *Environ. Pollut.* **1997**, *96*, 129−139. (b) Alvarez, E.; Fernandez-Marcos, M. L.; Monterroso, C.; Fernandez-Sanjurjo, M. J. Application of aluminium toxicity indices to soils under various forest species. *For. Ecol. Manage.* **2005**, *211*, 227−239. (c) Barcelo, J.; Poschenrieder, C. Fast root growth responses, root exudates, and internal detoxification as clues to the mechanisms of aluminium toxicity and resistance: a review. *Environ. Exp. Bot.* **2002**, *48*, 75−92.

(7) (a) Valeur, B.; Leray, I. Design principles of fluorescent molecular sensors for cation recognition. *Coord. Chem. Rev.* **2000**, *205*, 3−40. (b) Krejpcio, Z.; Wojciak, R. W. The Influence of Al^{3+} Ions on Pepsin and Trypsin Activity in Vitro. *Polym. J. Environ. Stud.* **2002**, *11*, 251−254.

(8) (a) Perl, D. P.; Gajdusek, D. C.; Garruto, R. M.; Yanagihara, R. T.; Gibbs, C. J. Intraneuronal aluminum accumulation in amyotrophic lateral sclerosis and Parkinsonism-dementia of Guam. *Science* **1982**, *217*, 1053−1055. (b) Perl, D. P.; Brody, A. R. Alzheimer's disease: X-ray spectrometric evidence of aluminum accumulation in neurofibrillary tangle-bearing neurons. *Science* **1980**, *208*, 297−299. (c) Altschuler, E. Aluminum-containing antacids as a cause of idiopathic Parkinson's disease. *Med. Hypotheses* **1999**, *53*, 22−23. (d) Shcherbatykh, I.; Carpenter, D. O. The role of metals in the etiology of Alzheimer's disease. *J. Alzheimer's Dis.* **2007**, *11*, 191−205.

(9) Exley, C.; Swarbrick, L.; Gherardi, R. K.; Authier, F. J. A role for the body burden of aluminium in vaccine-associated macrophagic myofasciitis and chronic fatigue syndrome. *Med. Hypotheses* **2009**, *72*, 135−139.

(10) (a) Soroka, K.; Vithanage, R.; Philips, D. A.; Walker, B.; Dasgupta, P. K. Fluorescence properties of metal complexes of 8-hydroxyquinoline-5-sulfonic acid and chromatographic applications. *Anal. Chem.* **1987**, *59*, 629−636. (b) Sun, X.; Wang, Y. W.; Peng, Y. A Selective and Ratiometric Bifunctional Fluorescent Probe for Al^{3+} Ion and Proton. *Org. Lett.* **2012**, *14*, 3420−3423.

(11) (a) Ghosh, K.; Majumdar, A.; Sarkar, T. Selective sensing of Al^{3+} by naphthyridine coupled rhodamine chemosensors. *RSC Adv.* **2014**, *4*, 23428−23432. (b) Maity, S. B.; Bharadwaj, P. K. A Chemosensor Built with Rhodamine Derivatives Appended to an Aromatic Platform via 1,2,3-Triazoles: Dual Detection of Aluminum(III) and Fluoride/Acetate Ions. *Inorg. Chem.* **2013**, *52*, 1161−1163. (c) Ding, P.; Wang, J.; Cheng, J.; Zhao, Y.; Ye, Y. Three N-stabilized rhodamine-based fluorescent probes for Al^{3+}*via* Al^{3+}-promoted hydrolysis of Schiff bases. *New J. Chem.* **2015**, *39*, 342−348. (d) Goswami, S.; Paul, S.; Manna, A. Selective "naked eye" detection of Al(III) and PPi in aqueous media on a rhodamine-isatin hybrid moiety. *RSC Adv.* **2013**, *3*, 10639−10643. (e) Jeong, J. W.; Rao, B. A.; Son, Y.-A. Rhodamine-chloronicotinaldehyde-based "OFF-ON" chemosensor for the colorimetric and fluorescent determination of Al^{3+}ions. *Sens. Actuators, B* **2015**, *208*, 75−84. (f) Mi, Y.-S.; Liang, D.-M.; Chen, Y.-T.; Luo, X.-B.;

DOI: 10.1021/acs.inorgchem.7b00835
Inorg. Chem. XXXX, XXX, XXX−XXX

Xiang, J.-N. A rhodamine-quinoline type molecular switch as a highly selective sequential sensor for Al^{3+} and F^- in aqueous solution. *RSC Adv.* **2014**, *4*, 42337−42345. (g) Chen, Y.; Mi, Y.; Xie, Q.; Xiang, J.; Fan, H.; Luo, X.; Xia, S. A new off-on chemosensor for Al^{3+} and Cu^{2+} in two different systems based on a rhodamine B derivative. *Anal. Methods* **2013**, *5*, 4818−4823. (h) Sen, B.; Mukherjee, M.; Banerjee, S.; Pal, S.; Chattopadhyay, P. A rhodamine-based 'turn-on' Al^{3+} ion-selective reporter and the resultant complex as a secondary sensor for F^- ion are applicable to living cell staining. *Dalton Trans.* **2015**, *44*, 8708−8717. (i) Kim, H.-S.; Angupillai, S.; Son, Y.-A. A dual chemosensor for both Cu^{2+} and Al^{3+}: A potential Cu^{2+} and Al^{3+} switched YES logic function with an INHIBIT logic gate and a novel solid sensor for detection and extraction of Al^{3+} ions from aqueous solution. *Sens. Actuators, B* **2016**, *222*, 447−458. (j) Qin, J.-C.; Yan, J.; Wang, B.; Yang, Z. Rhodamine-naphthalene conjugate as a novel ratiometric fluorescent probe for recognition of Al^{3+}. *Tetrahedron Lett.* **2016**, *57*, 1935−1939. (k) Ghosh, K.; Panja, S.; Sarkar, T. Rhodamine-linked pyridyl thiourea as a receptor for selective recognition of F^-, Al^{3+} and Ag^+ under different conditions. *Supramol. Chem.* **2015**, *27*, 490−500. (l) Fu, Y.; Jiang, X.-J.; Zhu, Y.-Y.; Zhou, B.-J.; Zang, S.-Q.; Tang, M.-S.; Zhang, H.-Y.; Mak, T. C. W. A new fluorescent probe for Al^{3+} based on rhodamine 6G and its application to bioimaging. *Dalton Trans.* **2014**, *43*, 12624−12632. (m) Kim, C.; Hwang, J.-Y.; Ku, K.-S.; Angupillai, S.; Son, Y.-A. A renovation of non-aqueous Al^{3+} sensor to aqueous media sensor by simple recyclable immobilize electrospun nano-fibers and its uses for live sample analysis. *Sens. Actuators, B* **2016**, *228*, 259−269.

(12) (a) Sun, Q.; Yan, B. Single bead IR monitoring of a novel benzimidazole synthesis. *Bioorg. Med. Chem. Lett.* **1998**, *8*, 361−364. (b) Madhu, S.; Sharma, D. K.; Basu, S. K.; Jadhav, S.; Chowdhury, A.; Ravikanth, M. Sensing Hg(II) in Vitro and in Vivo Using a Benzimidazole Substituted BODIPY. *Inorg. Chem.* **2013**, *52*, 11136−11145.

(13) Sigel, H.; McCormick, D. B. On the Discriminating behavior of metal ions and ligands with regard to their biological significance. *Acc. Chem. Res.* **1970**, *3*, 201−208.

(14) (a) Goswami, S.; Maity, S.; Maity, A. C.; Maity, A. K.; Das, A. K.; Saha, P. A FRET-based rhodamine-benzimidazole conjugate as a Cu^{2+}-selective colorimetric and ratiometric fluorescence probe that functions as a cytoplasm marker. *RSC Adv.* **2014**, *4*, 6300−6305. (b) Kar, C.; Adhikari, M. D.; Ramesh, A.; Das, G. NIR- and FRET-Based Sensing of Cu^{2+} and S^{2-} in Physiological Conditions and in Live Cells. *Inorg. Chem.* **2013**, *52*, 743−752. (c) Tang, L.; Li, F.; Liu, M.; Nandhakumar, R. A new rhodamine B derivative as a colorimetric chemosensor for recognition of Copper(II) ion. *Bull. Korean Chem. Soc.* **2010**, *31*, 3212−3216. (d) Li, J.; Hu, Q.; Yu, X.; Zeng, Y.; Cao, C.; Liu, X.; Guo, J.; Pan, Z. A novel rhodamine-benzimidazole conjugate as a highly selective turn-on fluorescent probe for Fe^{3+}. *J. Fluoresc.* **2011**, *21*, 2005−2013.

(15) Job, P. Formation and stability of inorganic complexes in solution. *Ann. Chim.* **1928**, *9*, 113−203.

(16) Valeur, B.; Pouget, J.; Bourson, J.; Kaschke, M.; Eensting, N. P. Tuning of photoinduced energy transfer in a bichromophoric coumarin supermolecule by cation binding. *J. Phys. Chem.* **1992**, *96*, 6545−6549.

(17) Caballero, A.; Martinez, R.; Lloveras, V.; Ratera, I.; Vidal-Gancedo, J.; Wurst, K.; Tarraga, A.; Molina, P.; Vaciana, J. Highly Selective Chromogenic and Redox or Fluorescent Sensors of Hg^{2+} in Aqueous Environment Based on 1,4-Disubstituted Azines. *J. Am. Chem. Soc.* **2005**, *127*, 15666−15667.

(18) Ghosh, K.; Sarkar, T. L-Valine derived benzimidazole based bis-urea in enantioselective fluorescence sensing of L-tartrate. *Tetrahedron Lett.* **2013**, *54*, 4568−4573.

(19) Ghosh, K.; Sarkar, T. Selective sensing of Cu (II) by a simple anthracene-based tripodal chemosensor. *Supramol. Chem.* **2011**, *23*, 435−440.

(20) (a) Kubin, R. F.; Fletcher, A. N. Fluorescence quantum yields of some rhodamine dyes. *J. Lumin.* **1982**, *27*, 455−462. (b) Wu, Y.; Peng, X.; Fan, J.; Gao, S.; Tian, M.; Zhao, J.; Sun, S. Fluorescence Sensing of Anions Based on Inhibition of Excited-State Intramolecular Proton Transfer. *J. Org. Chem.* **2007**, *72*, 62−70.

(21) *COLLECT, Program for Collecting Data on CCD Area Detectors*; Nonius BV, Delft, The Netherlands, 1998.

(22) Otwinowski, Z.; Minor, W. Processing of X-Ray Diffraction Data Collected in Oscillation Mode. *Methods Enzymol.* **1997**, *276*, 307−327.

(23) Otwinowski, Z.; Borek, D.; Majewski, W.; Minor, W. Multiparametric scaling of diffraction intensities. *Acta Crystallogr., Sect. A: Found. Crystallogr.* **2003**, *59*, 228−234.

(24) *APEX3, SADABS and SAINT*; Bruker AXS Inc., Madison, WI, USA, 2016.

(25) Sheldrick, G. M. SHELXT-Integrated space-group and crystal-structure determination. *Acta Crystallogr., Sect. A: Found. Adv.* **2015**, *71*, 3−8.

(26) Sheldrick, G. M. A short history of SHELX. *Acta Crystallogr., Sect. A: Found. Crystallogr.* **2008**, *64*, 112−122.

(27) *XP - Interactive molecular graphics, Version 5.1*, Bruker AXS Inc., Madison, WI, USA, 1998.

(28) (a) Zhao, Y.; Truhlar, D. G. Density Functionals with Broad Applicability in Chemistry. *Acc. Chem. Res.* **2008**, *41*, 157−167. (b) Zhao, Y.; Truhlar, D. G. Exploring the Limit of Accuracy of the Global Hybrid Meta Density Functional for Main-Group Thermochemistry, Kinetics, and Noncovalent Interactions. *J. Chem. Theory Comput.* **2008**, *4*, 1849−1868. (c) Hohenstein, E. G.; Chill, S. T.; Sherrill, C. D. Assessment of the Performance of the M05-2X and M06-2X Exchange-Correlation Functionals for Noncovalent Interactions in Biomolecules. *J. Chem. Theory Comput.* **2008**, *4*, 1996−2000.

(29) Zhao, Y.; Truhlar, D. The M06 Suite of Density Functionals for Main Group Thermochemistry, Thermochemical Kinetics, Noncovalent Interactions, Excited States, and Transition Elements: Two New Functionals and Systematic Testing of Four M06-Class Functionals and 12 Other Functionals. *Theor. Chem. Acc.* **2008**, *120*, 215−241.

(30) Frisch, M. J.; Trucks, G. W.; Schlegel, H. B.; Scuseria, G. E.; Robb, M. A.; Cheeseman, J. R.; Scalmani, G., et al. *Gaussian 09, Rev. B01*; Gaussian, Inc., Wallingford, CT, 2010.

DOI: 10.1021/acs.inorgchem.7b00835
Inorg. Chem. XXXX, XXX, XXX−XXX